Front. Phys. 13(5), 136802 (2018)
https://doi.org/10.1007/s11467-018-0769-z

REVIEW ARTICLE

Controlled growth of complex polar oxide films with atomically precise molecular beam epitaxy

Fang Yang[1], Yan Liang[1], Li-Xia Liu[1,2], Qing Zhu[1,2], Wei-Hua Wang[1], Xue-Tao Zhu[1,2], Jian-Dong Guo[1,2,3,†]

[1] *Beijing National Laboratory for Condensed Matter Physics & Institute of Physics, Chinese Academy of Sciences, Beijing 100190, China*
[2] *School of Physical Sciences, University of Chinese Academy of Sciences, Beijing 100049, China*
[3] *Collaborative Innovation Center of Quantum Matter, Beijing 100871, China*
Corresponding author. E-mail: †jdguo@iphy.ac.cn
Received January 8, 2018; accepted February 11, 2018

At heterointerfaces between complex oxides with polar discontinuity, the instability-induced electric field may drive electron redistribution, causing a dramatic change in the interfacial charge density. This results in the emergence of a rich diversity of exotic physical phenomena in these quasi-two-dimensional systems, which can be further tuned by an external field. To develop novel multifunctional electronic devices, it is essential to control the growth of polar oxide films and heterointerfaces with atomic precision. In this article, we review recent progress in control techniques for oxide film growth by molecular beam epitaxy (MBE). We emphasize the importance of tuning the microscopic surface structures of polar films for developing precise growth control techniques. Taking the polar $SrTiO_3$ (110) and (111) surfaces as examples, we show that, by keeping the surface reconstructed throughout MBE growth, high-quality layer-by-layer homoepitaxy can be realized. Because the stability of different reconstructions is determined by the surface cation concentration, the growth rate from the Sr/Ti evaporation source can be monitored in real time. A precise, automated control method is established by which insulating homoepitaxial $SrTiO_3$ (110) and (111) films can be obtained on doped metallic substrates. The films show atomically well-defined surfaces and high dielectric performance, which allows the surface carrier concentration to be tuned in the range of $\sim 10^{13}/cm^2$. By applying the knowledge of microstructures from fundamental surface physics to film growth techniques, new opportunities are provided for material science and related research.

Keywords complex oxide films, molecular beam epitaxy, surface reconstruction, heterointerfaces

PACS numbers 68.47.Gh, 68.35.B-, 77.55.Px, 68.55.-a, 81.15.-z

Contents

1 Introduction

Transition metal oxides (TMOs) have attracted extensive research interest owing to their rich phase diagram and unique properties. At TMO heterointerfaces, owing to the presence of broken symmetry, reduced dimensionality, and spatial confinement, even more exotic behav-

iors emerge that are related to, but distinct from, those in the bulk forms [1–4]. This offers great opportunities for next-generation all-oxide electronics because the low-dimensional electron systems hosted by TMO heterointerfaces are highly sensitive to external fields [5–8]. The essential basis of this field is precise control of the growth of TMO heterointerfaces. For example, it was reported that a two-dimensional electron gas (2DEG) appears at the interface between insulating $LaAlO_3$ and $SrTiO_3$ (STO) only when the STO substrate is terminated by a TiO_2 layer [2]. Further, both the electron density and electron mobility in the 2DEG are closely related to the quality of the heteroepitaxial films [9–11].

Great efforts have been made to obtain TMO films with precise stoichiometry [12–17]. Compared to the metal cations, the oxygen concentration is especially challenging to control due to its high vapor pressure and low adhesion efficiency, as well as the difficulty of *in situ* monitoring and post characterization. The oxygen concentration in TMO films is significantly influenced by the oxidant species (O, O_2, or O_3) and the corresponding partial pressure, the substrate temperature, and the annealing process. By carefully adjusting these growth parameters, the effect of oxygen vacancies (VOs) on the film properties has been investigated [18–24]. However, macroscopic tuning of the average chemical concentration cannot lead to a clear understanding of the underlying physics because in some cases VOs form clusters [25] and even induce phase separation in the system [26, 27]. It was also reported that lattice site occupation of cations affects the TMO properties [28–30]. In brief, it is extremely important to control the growth of TMO films at the atomic scale.

As typical correlated electron systems, many TMOs possess polarized bands with multiple degrees of freedom. Accordingly, different orders can be formed in the material when the electron density is varied. By exploiting the charge modulation at TMO heterointerfaces, multifunctional oxide devices can be realized [31–36]. One important issue is the investigation of polar TMO surfaces. As schematically shown in Fig. 1, the bulk truncated surface along the polar direction of an oxide is unstable. Dipoles are formed in adjacent layers with aligned orientation; thus, the electrostatic potential diverges with increasing thickness [Fig. 1(a)]. The macroscopic polarity can be canceled by modifying the charge density on both surfaces of the material as $\sigma' = \sigma d_2/(d_1 + d_2)$ [Fig. 1(b)]. Several mechanisms can change the surface charge density and compensate for the polarity, such as the formation of surface reconstruction and the adsorption of charged particles. At the interface between two oxides with different charge density in each layer, i.e., with polar discontinuity, charge transfer occurs, and the charge redistribution may reduce or even cancel the surface polarity. Most importantly, the density of the transferred charge can be extremely high (on the order of $10^{14}/\mathrm{cm}^2$, corresponding to ~ 1 electron per unit cell). Compared to tuning of the electric field in gate structures, the field can be tuned in a broad range at the atomic scale using heterointerfaces with polar discontinuity.

However, it is quite challenging to precisely control the growth of TMO heterostructures with polar dis-

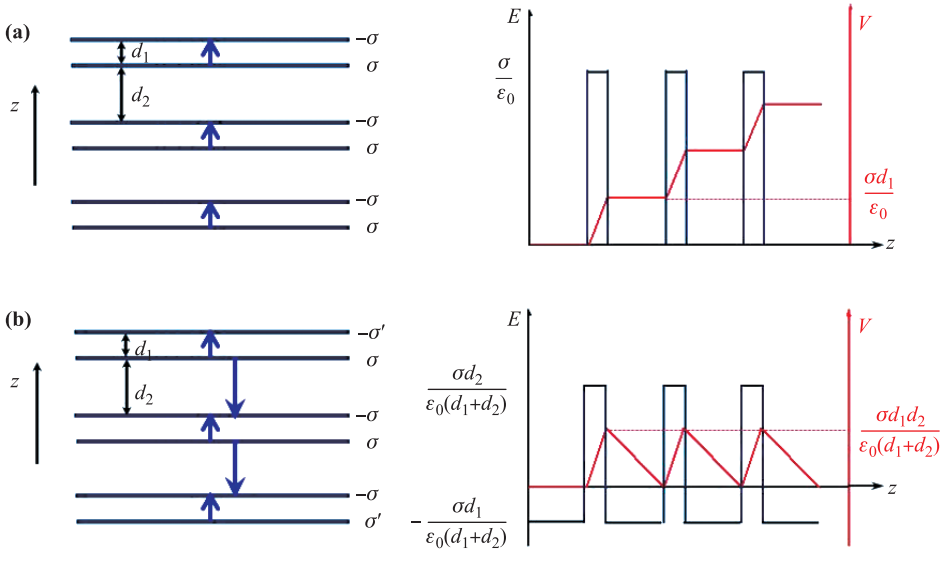

Fig. 1 Schematic diagram of the stabilization of polar surfaces. **(a)** Left panel: The polar surfaces have alternating net charges (σ) along z direction. Right panel: The presence of a non-zero dipole moment and the non-negative electric field (E) lead to an electric potential (V) diverging with thickness. **(b)** Left panel: Charge modulation occurs at the polar surface to cancel the polarity. Right panel: The electric field oscillates about zero and thus the electric potential remains finite.

continuity. In addition to the typical interfacial issues, e.g., chemical intermixing, elemental segregation, or defect trapping, polar instability often inhibits high-quality two-dimensional film growth. There have been reports that reconstructions can be formed on polar TMO surfaces during film growth by molecular beam epitaxy (MBE) [37–41]. Therefore, the polarity can be effectively compensated for and layer-by-layer growth enabled.

This article reviews relevant studies on the growth control of polar TMO films and heterointerfaces. Different reconstructions on the polar STO (110) and (111) surfaces and their stability are determined by the relative concentrations of Sr and Ti cations on the surface. Therefore, by keeping the film surface reconstructed during growth, the chemical stoichiometry can be monitored *in situ* and in real time by reflective high-energy electron diffraction (RHEED), which reveals not only the surface morphology but also the microstructure. Precise control techniques for MBE growth can be developed accordingly. The recent development of pulsed laser deposition (PLD) growth, which enables control of the growth kinetics of TMO heterointerfaces, is also introduced briefly.

2 Control techniques of chemical stoichiometry in oxide MBE

MBE has been employed to grow complex oxide films for 30 years, with the expectation of the same great success as that obtained for conventional semiconductors [42, 43]. However, unlike the self-regulated growth of GaAs, in which only one low-vapor-pressure element is involved and thus stoichiometry can be realized [44, 45], MBE growth of complex oxide films involves multiple metals with low vapor pressure, and precise control of each evaporation source is required. The quartz crystal microbalance (QCM) and atomic absorption spectroscopy (AAS) have been widely used for *in situ* calibration of the flux rates of metal evaporation beams. AAS usually supports composition control with better than 1% precision. However, it is not a real-time technique and cannot deal with random fluctuations during growth. Moreover, for some elements such as Ti, the absorption signal is too weak to detect, and the precision is far from satisfactory [12, 45]. Regarding the QCM, a large discrepancy might be introduced by the different adhesion coefficients of the quartz crystal and substrate owing to their different temperatures, chemical environments, and geometries with respect to the evaporation source.

In oxide MBE growth, the flux rate of a metal evaporation source varies in an uncontrolled way owing to its oxidation during growth (in oxygen ambient at high temperature). A specially designed geometry of the evaporation source and pumping scheme may reduce the change in the source rate [15, 46, 47]. A hybrid MBE technique, in which the metal sources are replaced by volatile metal-organic precursors, e.g., titanium tetra-isopropoxide or vanadium oxytriisopropoxide for Ti or V, respectively [48, 49], has also been introduced to avoid the oxidation problem. Nevertheless, the impurities introduced by the metal-organic precursor have not been investigated carefully yet, nor have the special growth dynamics and kinetics of hybrid MBE, which may cause phase limitation.

An *in situ*, real-time monitoring technique is imperative for control of the chemical stoichiometry in MBE growth. Indeed, RHEED has been demonstrated as an ideal tool, as its intensity responds sensitively to the morphology of the growing surface and reveals the growth mode and rate. Moreover, RHEED provides information on the surface microscopic structure and chemical concentration [12, 50–52], because the scattering matrix is determined by the mass and spatial arrangement of the scattering centers. By analyzing the fine structure of the RHEED intensity evolution during MBE growth of a STO (001) film, the cation stoichiometry can be optimized with a precision of 1% [12]. Recently, a particularly important control technique was developed on the basis of RHEED monitoring of the evolution of surface reconstructions with the cation concentration [37–39, 53–55]. Cation stoichiometry with a precision of ±0.3% was achieved in an STO (001) film grown on Si [37], and a precision of ±0.1% was demonstrated in a homoepitaxial STO (111) film [54]. With the advanced use of RHEED, control of oxide film growth can benefit dramatically from detailed knowledge of surface reconstructions.

3 Reconstructions of polar $SrTiO_3$ surfaces and their stability

Polar oxide surfaces exhibit high reconstruction instability [56]. Figure 2 shows two typical polar oxide surfaces, STO (110) and (111). Along the [110] direction, STO consists of stacks of alternating $(SrTiO)^{4+}/(O_2)^{4-}$ atomic layers, whereas along the [111] direction, it consists of stacks of $(SrO_3)^{4-}/(Ti)^{4+}$ atomic layers. Both surfaces are unstable owing to the aligned dipoles along the perpendicular direction. In the following, different reconstruction phases of polar STO surfaces and their evolution with the surface cation concentration will be introduced.

3.1 Reconstructions on $SrTiO_3$ (110)

A wide variety of reconstructions have been observed on the STO (110) surface, such as $(n \times 1)$ $(n = 3, 4, 6)$,

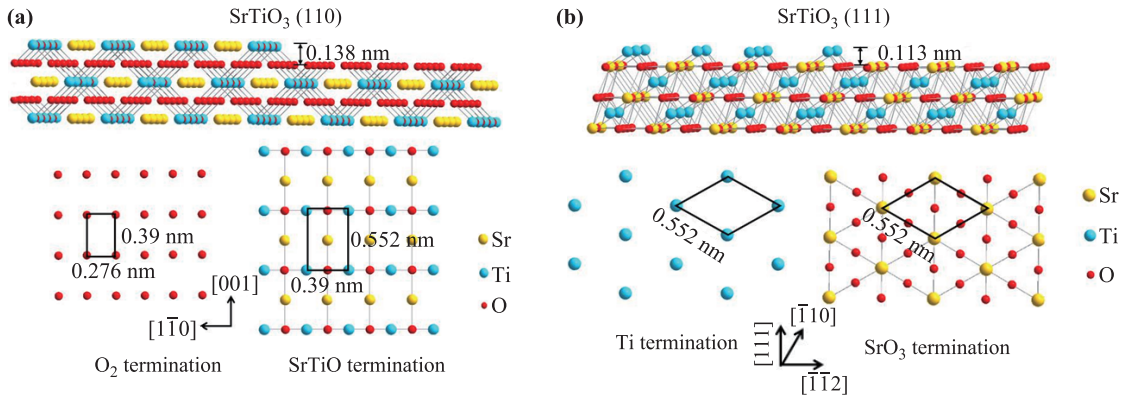

Fig. 2 Schematic drawings of the structures of bulk-truncated **(a)** $SrTiO_3$ (110) with $(SrTiO)^{4+}$ and $(O_2)^{4-}$ terminations, and **(b)** $SrTiO_3$ (111) with $(SrO_3)^{4-}$ and $(Ti)^{4+}$ terminations. The surface unit cells are labeled, respectively.

(2×5), (3×4), (4×4), (4×7), (6×4), (5×2), and $c(2 \times 6)$, depending on the preparation conditions [57–61]. Taking the (4×1) reconstruction as an example (top panel of Fig. 3), a scanning tunneling microscopy (STM) image shows periodic stripes along the $[1\bar{1}0]$ direction separated by dark trenches. This reconstructed structure corresponds to $(SrTiO)^{4+}$ termination [62]. Further study by STM combined with density functional theory (DFT) calculations, as discussed in detail below, resolves the atomistic structure, in which an adlayer of TiO_4 tetrahedra atop the $(SrTiO)^{4+}$ plane shares the corner oxygen that forms the (4×1) reconstruction on the STO (110) surface [57, 63]. The nominal chemical formula is $Ti_{1.5}O_4$ per (1×1) area on the topmost layer, which exhibits an extra charge of 2^- that satisfies the polar compensation criterion without varying the chemical valence of Ti.

Reconstructions of (5×1), (4×1), (2×8), or (6×8) can be obtained on STO (110) by Ar^+ sputtering followed by annealing in vacuum [62, 64]. As the sputtering dose is increased, the surface reconstruction is transformed gradually from SrTiO-terminated (5×1) to (4×1), then to O-terminated (2×8), and to (6×8), as shown in Fig. 3. Characterization of the nominal composition near the surface region by X-ray photoemission spectroscopy indicates a corresponding increase in the Ti/Sr concentration ratio. Note that these reconstructions are not oxygen-deficient; the oxygen concentration is higher than that on the cleaved STO (001) surface [64].

Alternatively, the reconstruction phases on STO (110) can be changed by Sr or Ti deposition followed by annealing [64]. The relative area ratio of adjacent phases can be continuously tuned by adjusting the deposition dosage, and monophased reconstructions can be obtained (see Fig. 3). For example, given the monophased (5×1) reconstruction as the starting surface, depositing a small amount of Ti (followed by annealing) induces the formation of (4×1) patches. With increasing Ti deposition dosage, the area of (4×1) is enlarged until a monophased (4×1) surface is obtained when 0.15 monolayer (ML) Ti is deposited on the (5×1) surface. The sharp fractional RHEED patterns shown in the bottom panel of Fig. 3 clearly indicate the phase transformation. As the Ti deposition dosage increases further, (2×8) and (6×8) reconstructions are developed sequentially. Further, this phase evolution can be reversed by depositing Sr with a dosage equivalent to that of Ti between adjacent phases in the opposite direction. The phase diagram of the STO (110) surface is shown in Fig. 3. All of the reconstruction phases are Ti-enriched. Owing to the high-temperature annealing (800°C), thermodynamic equilibrium is reached on the surface at any Sr/Ti concentration. Therefore, it is concluded that the stability of each

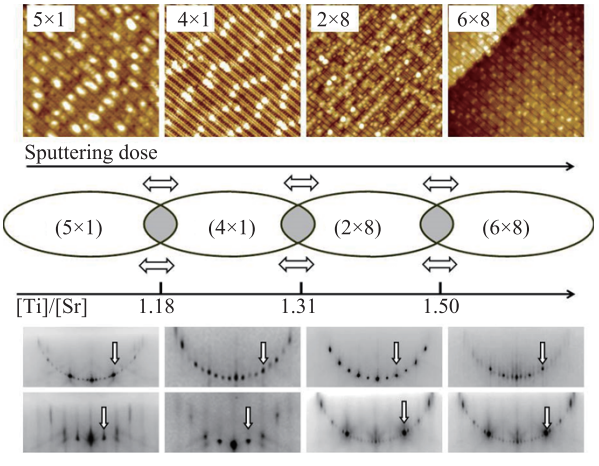

Fig. 3 The reversible transformation of different reconstruction phases on STO (110). Top panel (from left to right): STM images (30 nm × 30 nm, 20 pA/1.5 V) of (5×1), (4×1), (2×8), and (6×8). Middle panel: The phases diagram of STO (110) depending on the sputtering dose or the surface cation concentration. Bottom panel (from left to right): RHEED patterns along $[1\bar{1}0]$ (upper) and [001] (lower) directions [63].

reconstruction phase is determined by the cation concentration. Importantly, as observed by RHEED, a reconstruction with long-range periodicity can be formed even at a high annealing temperature [38].

3.2 Reconstructions on $SrTiO_3$ (111)

On another typical polar surface of STO, STO (111), a series of reconstructions have been observed, such as $(n \times n)$ $(n = 3$–$6)$, $(\sqrt{7} \times \sqrt{7})$–R19.1°, and $(\sqrt{13} \times \sqrt{13})$–R13.9°, depending on the treatment conditions [65–70]. Similar to those on the STO (110) surface, the reconstructions on STO (111) can also be reversibly modulated by Sr or Ti deposition followed by annealing [71]. Note that STO (111) is annealed under oxygen ambient with $P_{O2} = 5.5 \times 10^{-6}$ mbar, whereas STO (110) is annealed under ultrahigh vacuum (UHV). The reconstructed STO (111) surface can evolve from (4×4) to (6×6) and then to (5×5) reconstruction by increasing the Ti deposition dosage on the surface. Further, this evolution can be reversed by increasing the Sr deposition dosage. STM height analysis and the optimal evaporation dosage suggest that the (4×4) reconstructed structure corresponds to SrO_3 termination, whereas (6×6) and (5×5) correspond to Ti termination.

As shown in the top panel of Fig. 4, the (4×4) reconstruction features bright three-blade shapes with chirality arranged in the (4×4) hexagonal lattice. The unit cell of the (6×6) reconstruction is composed of a bright triangle and a bright dot. Similarly, the (5×5) reconstruction also consists of two triangular parts; one exhibits a bright dot in the center, and the other shows a dark center.

Although Russell and Castell have classified the (4×4), (6×6), and (5×5) reconstructions into a single family of $(n \times n)$ reconstructions [70], the three reconstructions may have different polar compensation mechanisms, and their absorption behaviors are quite different. A clean (4×4) reconstruction is difficult to obtain; i.e., it is always covered by triangular adsorbates (a minimum of $\sim 28\%$ in area). These disordered adsorbates might contribute to polar compensation along with reconstruction. In contrast, the monophased (6×6) reconstruction can be obtained, indicating that the (6×6) reconstruction itself is polar-compensated. For the (5×5) reconstruction, Russell and Castell obtained a flat surface; however, Feng *et al.* found that it tends to form three-dimensional islands, because it may be unstable in oxygen ambient, and thus the surface tends to be rough [71].

Notably, just as in the case of STO (110), both the evolution of the reconstructions on STO (111) and their stability depend on the Sr/Ti ratio, and these reconstructions can form at high temperature. The RHEED patterns shown in the bottom panel of Fig. 4 distinctly reveal the reconstruction evolution among (4×4), (6×6), and (5×5) induced by Ti or Sr deposition.

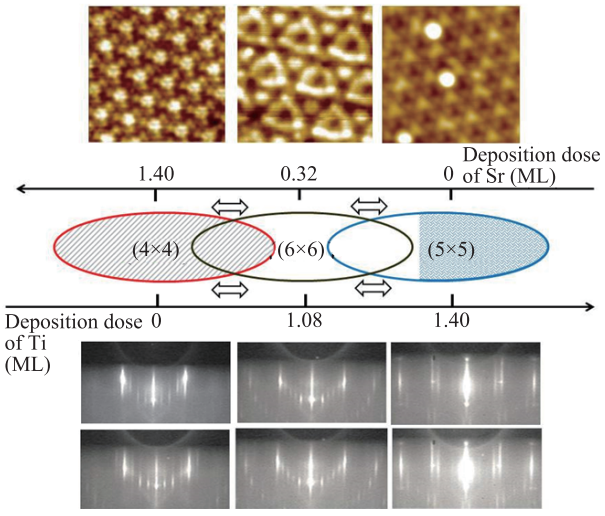

Fig. 4 The reversible transformation between different reconstructions on STO (111) surface. Top panel (from left to right): STM images (40 pA/2.3 V) of the reconstructions of (4×4) (12 nm × 12 nm), (6×6) (10 nm × 10 nm), and (5×5) (15 nm × 15 nm), respectively. Middle panel: The surface evolution of STO (111) depending on the deposition dosage of Sr or Ti. The shaded area in the (4×4) region indicates the existence of the triangular adsorbates, while the shaded area in the (5×5) region indicates the existence of multilayered islands. Bottom panel (from left to right): RHEED patterns along $[1\bar{1}0]$ (upper) and $[\bar{2}11]$ (lower) directions.

3.3 Atomistic structures resolved by a combination of experiments and calculations

The atomistic structures of reconstructions on polar STO (110) surfaces can be resolved by a combination of STM and *ab initio* calculations using DFT. As proposed by Enterkin *et al.* [57], the (3×1) reconstruction consists of rings of six or eight corner-sharing TiO_4 tetrahedra. The structure can be extended to a homologous series of $(n \times 1)$ atomistic reconstruction structures $(2 \leq n \leq 6$ and $n = \infty)$. The size of the large ring consisting of TiO_4 tetrahedra is enlarged by inserting an extra tetrahedron as n increases. Further, all the $(n\times1)$ reconstructions are charge-compensated with nominal surface compositions of $[Ti_{(n+2)/n}O_{(3n+4)/n}]^{2-}$ per (1×1) unit cell. Compared with the experimental results, the (4×1) reconstruction agrees well with such atomistic structural model, as shown in the left panel of Fig. 5. However, the simulated STM images of the (5×1) reconstruction based on this model are not fully consistent with the experimental features. To fit the experimental results, as shown in Fig. 5(b), TiO_4 tetrahedron 1 should be shifted from the linear chain along [001] to the middle of the zigzag chain along $[1\bar{1}0]$ [63]. The simulated STM image of the

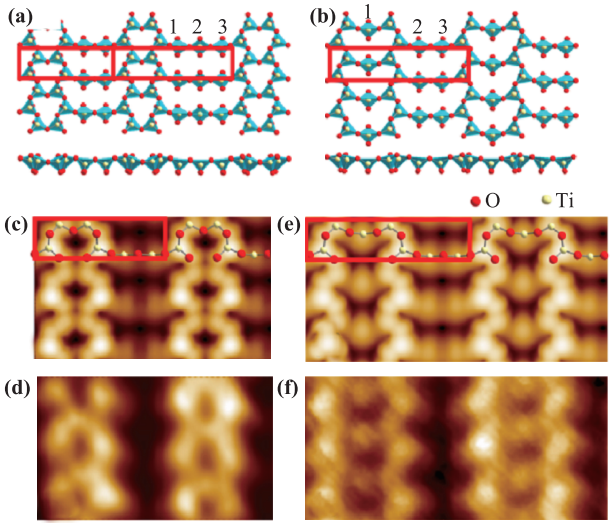

Fig. 5 **(a)** Structural model of the $(n \times 1)$ reconstruction with (4×1) on the left and (5×1) on the right. **(b)** The modified structural model of (5×1). The upper panels are the top view while the lower panels are the side view. **(c, d)** and **(e, f)** The simulated and experimental STM images of (4×1) and (5×1), respectively [63].

structure after relaxation reproduces the experimental characteristics excellently [Figs. 5(e) and (f)].

Studying the atomistic structure is helpful for quantitative analysis of the RHEED patterns and their intensity at the level of the scattering matrix [39]. Furthermore, learning the energy configuration of different reconstructions is also essential to establishing the growth control method. In oxides, specifically, the oxygen chemical potential is related to, or even determined by, the energy configuration of cations in thermodynamic equilibrium. If the metal stoichiometry is well controlled during growth, one can obtain high-quality films even when VOs are eliminated at a low growth rate and high temperature [72–76].

Calculations of the formation energy of VOs on different layers of STO (110) show that, owing to the energy configuration associated with surface reconstruction, all of the VOs are confined within a few subsurface layers. On the other hand, thermodynamics and kinetics studies of the atomistic surface processes during film growth indicate that the cation diffusion barrier to form reconstructions on the surface is much higher than that of oxygen diffusion toward the surface. Therefore, STO (110) polar films with high quality and low VO density can be grown by MBE even in UHV [77]. Moreover, a quasi-two-dimensional VO-doped region forms, similar to the case of δ-doping in conventional semiconductors. The charge density of such a δ-doping layer can be precisely controlled because the total VO population can be tuned using the oxygen chemical potential during preparation.

Similarly, reconstructions on the STO (111) surface such as the $(n \times n)$ $(2 \leq n \leq 4)$ reconstructions are also considered as a network of TiO_4 tetrahedra on the (110) surface residing on octahedral TiO_5 with a vacant oxygen site and TiO_6 octahedra in the second layer [78]. The anatase TiO_2 (101) surface exhibits a similar characteristic [79]. These results open a new way to resolving the difficulty in controlling or minimizing the VO density to obtain an oxide surface or other low-dimensional structure with ideal stoichiometry.

4 Precise control of film growth by monitoring the evolution of surface reconstructions

Because the stability of reconstructions on polar STO surfaces is determined by the cation concentration, and the reconstructions can be detected *in situ* and in real time at high temperatures, monitoring their evolution may provide a signal for precise control of MBE growth of high-quality films. The presupposition is that the thermodynamics should play an important role. Of course, it is also a critical issue whether the cation nonstoichiometry exists only on the surface. For $BaTiO_3$ films grown on a $SrRuO_3$ substrate, the reconstruction of $SrRuO_3$ was considered to be buried under the $BaTiO_3$ film [80]. However, for other oxides such as STO, a transmission electron microscopy (TEM) study and DFT calculations verified that the reconstruction can exist only on the surface [61].

Homoepitaxial STO (110) films have been grown by coevaporating Sr and Ti in oxygen under precise control [38]. Although the flux rates of the source metals were calibrated by a QCM before MBE growth, the RHEED intensity oscillation faded out after the growth of a few layers, indicating failure of high-quality two-dimensional growth. On the other hand, it is observed that the RHEED patterns evolve from "1×" to weak "8×" [Figs. 6(a)–(c)]. These results demonstrate that the evaporation rates of the Sr and Ti sources are not exactly the same, and the discrepancy accumulates on the top few layers of the growing film. This accumulation, which is reflected by the RHEED patterns, provides high sensitivity that enables precise control of the polar film growth *in situ* and in real time. In this case, one can adjust the flux rate by varying either the source temperature or evaporation time until the RHEED pattern remains unchanged during extended growth. Thus, stable layer-by-layer growth is realized, as demonstrated by the significantly improved RHEED oscillations [Figs. 6(d)–(f)]. The high quality of the film is revealed by STM and high-resolution cross-sectional TEM images [Figs. 6(g), (h)]. As shown in Fig. 6(h), the interface between the

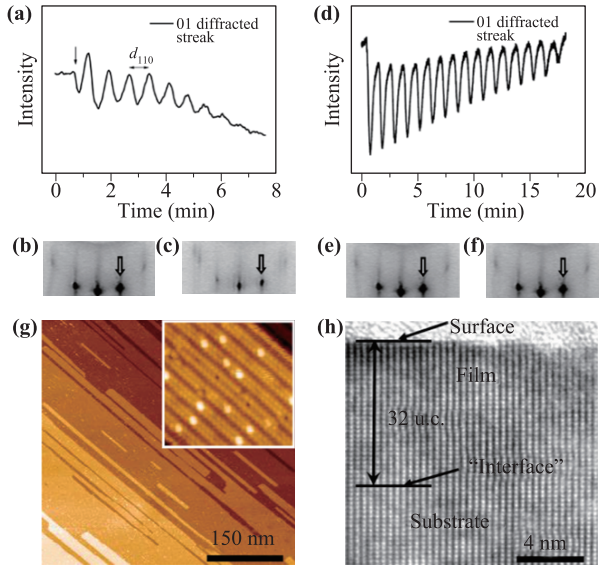

Fig. 6 **(a)** The RHEED intensity oscillations of the (01) pattern during the OMBE growth of STO (110) film after calibrating the flux rates of sources by QCM. **(b, c)** RHEED patterns along [1$\bar{1}$0] observed at the growth time of 0 (the substrate) and 7 min, respectively. The (01) patterns are indicated with arrows. **(d)** The RHEED intensity oscillations of the (01) pattern during growth after optimizing the temperature of evaporation sources. **(e, f)** RHEED patterns along [1$\bar{1}$0] observed at the growth time of 0 (the substrate) and 18 min, respectively. **(g)** STM image (2.0 V/50 pA) of an as-grown surface of 32-unit-cell-thick film. The inset shows the high resolution image. **(h)** Cross-sectional TEM image of the homoepitaxial STO (110) film. The interface is indistinguishable and it is determined by counting atomic layers from the film surface [38].

substrate and the homoepitaxial film cannot be identified, suggesting that the film lattice is perfect. The precision of the cation stoichiometry is better than 0.5%, as determined by energy dispersion spectroscopy [38]. Note that the accumulation effect is important for improving the precision of stoichiometry control. Owing to the limited RHEED sensitivity, it takes a long time to accumulate a detectable discrepancy in the cation concentrations; i.e., as the calibration duration increases, the precision of the stoichiometry could increase.

An automatic control technique with atomic precision has been further developed for MBE growth of STO (110) films [39]. Instead of the fractional RHEED patterns, of which the intensity variation becomes detectable as stoichiometric drift accumulates, the integral patterns are monitored and taken as the control signal. By using a kinematic model in the single-scattering limit [51, 81] and taking the atomistic structural model of STO (110)-($n \times 1$) from DFT calculations and the atomic scattering factor [81], the dependence of the integral RHEED patterns of the surface reconstruction or roughness on the incident angle of the electron beam (θ_i) is analyzed. When $\theta_i \approx 1.8°$, the RHEED intensity is much more sensitive to the surface reconstruction (i.e., the surface cation concentration) than the roughness (at the scale of unit cells). Technically, the incident angle of the electron beam can be adjusted within the grazing range, so the variation of the surface chemical concentration is sensitively represented by the intensity change of the integral RHEED patterns, which is monitored as the automatic feedback control signal to switch the status of the source shutter in real time. When the RHEED intensity drops (indicating that the growing surface becomes Sr-rich) by a certain amount, the shutter of the Sr source is closed automatically, whereas when the RHEED intensity increases, it is opened. Homoepitaxy can be achieved by keeping the reconstruction evolution within the reversible range. This precise method eliminates the uncontrollable fluctuation of the source flux and can be used to grow films with a desired thickness.

To maintain the reconstructions on polar surfaces, the oxide MBE method generally requires a high growth temperature. Consequently, in most cases, the oxygen pressure during growth also needs to be high to prevent decomposition of oxide materials and to obtain the expected phase [82, 83]. Although this might raise the risk of inducing cation interdiffusion across the interface [84–86], there have been examples of its successful application to heteroepitaxy. Li *et al.* obtained high-quality heteroepitaxial $LaTiO_3$ (110) films by keeping the growing surface reconstructed in (2×16) [87]. The intensity of the RHEED patterns, either the integral or fractional patterns, exhibits behavior quite similar to that in homoepitaxial growth. The only difference from homoepitaxy is that 2 ML La and Ti should be deposited first onto the STO (110) substrate surface to form the (2×16) reconstruction as the initial surface.

Polar oxide surfaces along the [111] direction offer even more flexible tunability of the physical properties [88, 89]. The double-perovskite structure $A_2BB'O_6$ can be artificially constructed as the [111]-oriented superlattice $AO_3/B/AO_3/B'$. Further, the six-fold symmetry might lead to the formation of novel quantum states such as half-metallic ferromagnetism or the quantum anomalous Hall effect [90–96]. Dielectric STO (111) films have been homoepitaxially grown on metallic Nb-doped STO substrates by a similar feedback control method, as described above [54]. The films, which have atomically well-defined surfaces, show high dielectric performance, and the charge density is tunable in the range of $2 \times 10^{13}/cm^2$ with a back gate voltage lower than 0.2 V. Figure 7(a) shows a schematic of the setup for dielectric property measurement. The leakage current density of films at different electric fields is shown in

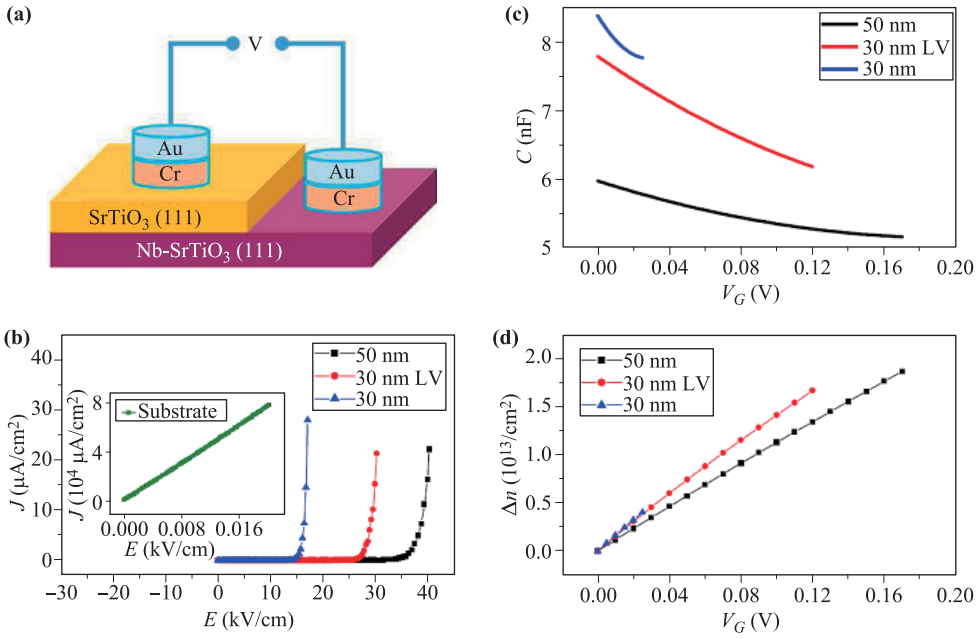

Fig. 7 **(a)** The schematic drawing of the Au/Cr/STO/Nb-STO capacitor structure. **(b)** The leakage current density at different electric field, **(c)** the capacitance at different bias, and **(d)** the charge density modulation range with different gate voltage measured at 6 K, respectively [54].

Fig. 7(b). It remains extremely low (< 1 μA/cm^2) until the electric field reaches the breakdown value. The capacitance measured at various gate voltages is displayed in Fig. 7(c), where the charge modulation Δn can be determined. Figure 7(d) shows the dependence of Δn upon the gate voltage, which must be below the breakdown field, suggesting that Δn can be effectively enhanced by reducing the VO concentration. The STO (111) film with an atomically well-defined surface and remarkable dielectric properties provides an ideal platform for epitaxy of novel quantum materials as well as control of the electronic properties of their device structures.

5 Control of the growth kinetics in pulsed laser deposition

By the method described above, complex polar oxide films can be epitaxially grown by MBE under precise control. However, as mentioned above, this requires a very high substrate temperature for the formation of surface reconstructions, which inevitably enables chemical intermixing and might degrade the sharpness of the heterointerface. It is essential that the growth kinetics play a more important role than the thermodynamics during the growth of these artificial low-dimensional systems. Increasing the growth rate is apparently an effective method. Unlike the case of growth by MBE, where the growth rate is limited by the use of metal sources with low vapor pressure, the growth rate is much more flexible in growth by PLD.

Recently, PLD in UHV chambers has been combined with RHEED, making it a powerful technique for precisely controlled growth of TMO films [1, 2, 97]. Although it is commonly believed that PLD provides nearly stoichiometric composition transfer from the target to the film [98], the growth of polar films is still a challenge. A simple method to consider is to circumvent the polar catastrophe, i.e., to grow polar films with continuous polarity at the interfaces. For example, selecting a suitable substrate or growing a buffer layer with the same polarity as the polar films can efficiently prevent the electronically active multivalent ions from changing the valence [99]. Because electronic reconstruction facilitates polar compensation without necessitating intermixing, introducing a metallic screening layer would also be effective. Using a conducting buffer layer on the polar substrate surface, Blok *et al.* succeeded in epitaxially growing $BiFeO_3$ and $CaTiO_3$ films on $SrTiO_3$ and $LaAlO_3$, respectively [100]. Similarly, Mukunoki *et al.* deposited a very thin, oxygen-deficient homoepitaxial STO (110) layer before heteroepitaxy so that the VOs in the initial buffer layer could compensate for the charges transferred between the film and substrate [101].

A general control method for PLD growth of polar TMO films and heterointerfaces was developed by Koster *et al.* [102]. They used a rather high laser frequency (as high as 100 Hz) to deposit one ML's worth of mate-

rial in a very short time and then used a much longer interval to rearrange the film lattice. Using this so-called interrupted growth method, they obtained STO homoepitaxial films and $[BaCuO_2/SrCuO_2]_n$ superlattices. Chakhalian's group succeeded in achieving layer-by-layer growth of nickelates. As the pulse frequency increases to 30 Hz, it exhibits a quasi-constant state with an average high flux. During the short deposition intervals, only small islands are formed owing to the high supersaturation. As the average radius of the islands decreases, nucleation of the islands becomes less probable. Supersaturation is far from the equilibrium state, and the nucleation barrier is overcome only during the long intervals of rearrangement, resulting in rapid nucleation from the supercritical vapor [103]. Consequently, the substrate temperature in interrupted growth can be low, which prevents interdiffusion across the heterointerface. This interval growth technique is unique to PLD; no other technique can combine very high deposition rates with intervals of no deposition in a fast periodic sequence [102].

Last but not least, it has been determined that the growth parameters of PLD, e.g., the laser energy density, growth temperature, and oxygen pressure, do affect the film stoichiometry. For example, one cannot obtain stoichiometric films if the laser energy density is below a threshold fluence value [104]. In this regard, keeping the surface reconstruction, which can be monitored by RHEED, unchanged throughout the growth process might also be critical for precise control of the stoichiometry and high-quality layer-by-layer growth of polar oxide films by PLD. Indeed, high-quality heteroepitaxy has been achieved on the reconstructed surface [105].

6 Conclusions

Research on emergent phenomena at heterointerfaces between complex oxides with polar discontinuity is a rapidly advancing field. Exploiting and understanding the underlying physics are necessary for precise growth control of polar films. We review recent progress in control techniques for polar oxide film growth by MBE. Although MBE is a typical kinetic growth process, it somehow allows the thermodynamics to play an important role. We highlight the importance of knowing the microscopic surface structures on polar films for establishing reliable precise growth control techniques. Taking the STO (110) and (111) surfaces as examples, we show that the surface polarity can be compensated for by the formation of reconstructions. Therefore, high-quality two-dimensional growth of polar films is realized by keeping the surface reconstructed throughout the growth process. Further, the fact that the stability of different reconstructions is determined by the surface cation concentration enables real-time monitoring of the growth rate of each metal source. A precise, *in situ*, and automated control method has been developed, and high-quality homoepitaxial layers of STO (110) and STO (111) have been obtained on doped metallic substrates. By applying the knowledge of microstructures from fundamental surface physics to film growth techniques, new opportunities for designing complex superlattices and heterointerfaces with rich controllable functionalities become available.

Acknowledgements This work was supported by the National Natural Science Foundation of China (Grant Nos. 11474334, 11634016, and 11404381), the National Key R&D Program of the Ministry of Science and Technology of China (Grant Nos. 2017YFA0303600 and 2014CB921001), the Open Research Fund Program of the State Key Laboratory of Low-Dimensional Quantum Physics, and the Strategic Priority Research Program (B) of the Chinese Academy of Sciences (Grant No. XDB07030100).

References

1. A. Ohtomo, D. A. Muller, J. L. Grazul, and H. Y. Hwang, Artificial charge-modulation in atomic-scale perovskite titanate superlattices, *Nature* 419(6905), 378 (2002)
2. A. Ohtomo and H. Y. Hwang, A high-mobility electron gas at the $LaAlO_3/SrTiO_3$ heterointerface, *Nature* 427(6973), 423 (2004); corrigendum: *Nature* 441(7089), 120 (2006)
3. A. Gozar, G. Logvenov, L. F. Kourkoutis, A. T. Bollinger, L. A. Giannuzzi, D. A. Muller, and I. Bozovic, High-temperature interface superconductivity between metallic and insulating copper oxides, *Nature* 455(7214), 782 (2008)
4. H. Y. Hwang, Y. Iwasa, M. Kawasaki, B. Keimer, N. Nagaosa, and Y. Tokura, Emergent phenomena at oxide interfaces, *Nat. Mater.* 11(2), 103 (2012)
5. Y. W. Xie, C. Bell, Y. Hikita, and H. Y. Hwang, Tuning the electron gas at an oxide heterointerface via free surface charges, *Adv. Mater.* 23(15), 1744 (2011)
6. A. D. Caviglia, S. Gariglio, N. Reyren, D. Jaccard, T. Schneider, M. Gabay, S. Thiel, G. Hammerl, J. Mannhart, and J.M. Triscone, Electric field control of the $LaAlO_3/SrTiO_3$ interface ground state, *Nature* 456(7222), 624 (2008)
7. C. Cen, S. Thiel, G. Hammerl, C. W. Schneider, K. E. Andersen, C. S. Hellberg, J. Mannhart, and J. Levy, Nanoscale control of an interfacial metal-insulator transition at room temperature, *Nat. Mater.* 7(4), 298 (2008)
8. S. Mathews, R. Ramesh, T. Venkatesan, and J. Benedetto, Ferroelectric field effect transistor based

on epitaxial perovskite heterostructures, *Science* 276(5310), 238 (1997)

9. W. Siemons, G. Koster, H. Yamamoto, W. A. Harrison, G. Lucovsky, T. H. Geballe, D. H. A. Blank, and M. R. Beasley, Origin of charge density at $LaAlO_3$ on $SrTiO_3$ heterointerfaces: Possibility of intrinsic doping, *Phys. Rev. Lett.* 98(19), 196802 (2007)
10. D. G. Schlom and L. N. Pfeiffer, Oxide electronics: Upward mobility rocks! *Nat. Mater.* 9(11), 881 (2010)
11. Z. Q. Liu, C. J. Li, W. M. Lü, X. H. Huang, Z. Huang, S. W. Zeng, X. P. Qiu, L. S. Huang, A. Annadi, J. S. Chen, J. M. D. Coey, T. Venkatesan, and Ariando, Origin of the two-dimensional electron gas at $LaAlO_3/SrTiO_3$ interfaces: The role of oxygen vacancies and electronic reconstruction, *Phys. Rev. X* 3(2), 021010 (2013)
12. J. H. Haeni, C. D. Theis, and D. G. Schlom, RHEED intensity oscillations for the stoichiometric growth of $SrTiO_3$ thin films by reactive molecular beam epitaxy, *J. Electroceram.* 4(2–3), 385 (2000)
13. A. Tselev, P. Ganesh, L. Qiao, W. Siemons, Z. Gai, M. D. Biegalski, A. P. Baddorf, and S. V. Kalinin, Oxygen control of atomic structure and physical properties of $SrRuO_3$ surfaces, *ACS Nano* 7(5), 4403 (2013)
14. S. Y. Jang, S. J. Moon, B. C. Jeon, and J. S. Chung, PLD growth of epitaxially-stabilized 5d perovskite $SrIrO_3$ thin films, *J. Korean Phys. Soc.* 56(6), 1814 (2010)
15. Y. S. Kim, N. Bansal, C. Chaparro, H. Gross, and S. Oh, Sr flux stability against oxidation in oxide-molecular-beam-epitaxy environment: Flux, geometry, and pressure dependence, *J. Vac. Sci. Technol. A* 28(2), 271 (2010)
16. H. M. Christen, L. A. Boatner, J. D. Budai, M. F. Chisholm, L. A. Gea, P. J. Marrero, and D. P. Norton, The growth and properties of epitaxial $KNbO_3$ thin films and $KNbO_3/KTaO_3$ superlattices, *Appl. Phys. Lett.* 68(11), 1488 (1996)
17. H. J. Bae, J. Sigman, S. J. Park, Y. H. Heo, L. A. Boatner, and D. P. Norton, Growth of semiconducting $KTaO_3$ thin films, *Solid-State Electron.* 48(1), 51 (2004)
18. Z. L. Liao, F. M. Li, P. Gao, L. Li, J. D. Guo, X. Q. Pan, R. Jin, E. W. Plummer, and J. D. Zhang, Origin of the metal-insulator transition in ultrathin films of $La_{2/3}Sr_{2/3}MnO_3$, *Phys. Rev. B* 92(12), 125123 (2015)
19. Z. P. Li, M. Bosman, Z. Yang, P. Ren, L. Wang, L. Cao, X. Yu, C. Ke, M. B. H. Breese, A. Rusydi, W. Zhu, Z. Dong, and Y. L. Foo, Interface and surface cation stoichiometry modified by oxygen vacancies in epitaxial manganite films, *Adv. Funct. Mater.* 22(20), 4312 (2012)
20. W. S. Choi, C. M. Rouleau, S. S. A. Seo, Z. Luo, H. Zhou, T. T. Fister, J. A. Eastman, P. H. Fuoss, D. D. Fong, J. Z. Tischler, G. Eres, M. F. Chisholm, and H. N. Lee, Atomic layer engineering of perovskite oxides for chemically sharp heterointerfaces, *Adv. Mater.* 24(48), 6423 (2012)
21. B. Stanka, W. Hebenstreit, U. Diebold, and S. A. Chambers, Surface reconstruction of $Fe_3O_4(001)$, *Surf. Sci.* 448(1), 49 (2000)
22. P. K. Nayak, M. N. Hedhili, D. K. Cha, and H. N. Alshareef, High performance solution-deposited amorphous indium gallium zinc oxide thin film transistors by oxygen plasma treatment, *Appl. Phys. Lett.* 100(20), 202106 (2012); *errutum: Appl. phys. Lett.* 105(24), 249902 (2014)
23. C. K. Tan, G. K. L. Goh, and W. L. Cheah, Dielectric properties of hydrothermally epitaxied *I–V* perovskite thin films, *Thin Solid Films* 515(16), 6577 (2007)
24. T. S. Herng, S. P. Lau, S. F. Yu, H. Y. Yang, K. S. Teng, and J. S. Chen, Enhancement of ferromagnetism and stability in Cu-doped ZnO by N_2O annealing, *J. Phys.: Condens. Matter* 19(35), 356214 (2007)
25. D. A. Muller, N. Nakagawa, A. Ohtomo, J. L. Grazul, and H. Y. Hwang, Atomic-scale imaging of nanoengineered oxygen vacancy profiles in $SrTiO_3$, *Nature* 430(7000), 657 (2004)
26. L. D. Yao, S. Inkinen, and S. van Dijken, Direct observation of oxygen vacancy-driven structural and resistive phase transitions in $La_{2/3}Sr_{1/3}MnO_3$, *Nat. Commun.* 8, 14544 (2017)
27. F. Lichtenberg, D. Widmer, J. G. Bednorz, T. Williams, and A. Reller, Phase-diagram of latiox - from 2d layered ferroelectric insulator to 3d weak ferromagnetic semiconductor, *Z. Phys. B - Condensed Matter* 82(2), 211 (1991)
28. M. Choi, F. Oba, and I. Tanaka, Role of Ti antisite-like defects in $SrTiO_3$, *Phys. Rev. Lett.* 103(18), 185502 (2009)
29. F. Yang, Q. Zhang, Z. Yang, J. Gu, Y. Liang, W. Li, W. Wang, K. Jin, L. Gu, and J. Guo, Room-temperature ferroelectricity of $SrTiO_3$ films modulated by cation concentration, *Appl. Phys. Lett.* 107(8), 082904 (2015)
30. E. Breckenfeld, N. Bronn, J. Karthik, A. R. Damodaran, S. Lee, N. Mason, and L. W. Martin, Effect of growth induced (non) stoichiometry on interfacial conductance in $LaAlO_3/SrTiO_3$, *Phys. Rev. Lett.* 110(19), 196804 (2013)
31. H. Yamada, M. Kawasaki, T. Lottermoser, T. Arima, and Y. Tokura, $LaMnO_3/SrMnO_3$ interfaces with coupled charge-spin-orbital modulation, *Appl. Phys. Lett.* 89(5), 052506 (2006)
32. N. Nakagawa, H. Y. Hwang, and D. A. Muller, Why some interfaces cannot be sharp, *Nat. Mater.* 5(3), 204 (2006)
33. J. Chakhalian, J. W. Freeland, A. J. Millis, C. Panagopoulos, and J. M. Rondinelli, Emergent properties in plane view: Strong correlations at oxide interfaces, *Rev. Mod. Phys.* 86(4), 1189 (2014)
34. S. Okamoto and A. J. Millis, Electronic reconstruction at an interface between a Mott insulator and a band insulator, *Nature* 428(6983), 630 (2004)

35. J. Chakhalian, J. W. Freeland, H. U. Habermeier, G. Cristiani, G. Khaliullin, M. van Veenendaal, and B. Keimer, Orbital reconstruction and covalent bonding at an oxide interface, *Science* 318(5853), 1114 (2007)

36. Q. Y. Wang, Z. Li, W.H. Zhang, Z.C. Zhang, J.S. Zhang, W. Li, H. Ding, Y.B. Ou, P. Deng, K. Chang, J. Wen, C.L. Song, K. He, J.F. Jia, S.H. Ji, Y.Y. Wang, L.L. Wang, X. Chen, X.C. Ma, and Q.K. Xue, Interface-induced high-temperature superconductivity in single unit-cell FeSe films on $SrTiO_3$, *Chin. Phys. Lett.* 29(3), 037402 (2012)

37. M. P. Warusawithana, C. Cen, C. R. Sleasman, J. C. Woicik, Y. Li, L. F. Kourkoutis, J. A. Klug, H. Li, P. Ryan, L.P. Wang, M. Bedzyk, D. A. Muller, L.Q. Chen, J. Levy, and D. G. Schlom, A ferroelectric oxide made directly on silicon, *Science* 324(5925), 367 (2009)

38. Z. M. Wang, J. G. Feng, Y. Yang, Y. Yao, L. Gu, F. Yang, Q. L. Guo, and J. D. Guo, Cation stoichiometry optimization of SrTiO3 (110) thin films with atomic precision in homogeneous molecular beam epitaxy, *Appl. Phys. Lett.* 100(5), 051602 (2012)

39. J. G. Feng, F. Yang, Z. M. Wang, Y. Yang, L. Gu, J. D. Zhang, and J. D. Guo, Growth of $SrTiO_3$ (110) film by oxide molecular beam epitaxy with feedback control, *AIP Adv.* 2(4), 041407 (2012)

40. S. Phark, Y. J. Chang, and T. Won Noh, Selective growth of perovskite oxides on $SrTiO_3$ (001) by control of surface reconstructions, *Appl. Phys. Lett.* 98(16), 161908 (2011)

41. Y. J. Chang and S. H. Phark, Atomic-scale visualization of initial growth of perovskites on $SrTiO_3$(001) using scanning tunneling microscope, *Curr. Appl. Phys.* 17(5), 640 (2017)

42. R. A. Betts and C. W. Pitt, Growth of thin-film lithium-niobate by molecular-beam epitaxy, *Electron. Lett.* 21(21), 960 (1985)

43. M. Petrucci, C. W. Pitt, and P. J. Dobson, RHEED studies on Z-cut $LiNbO_3$, *Electron. Lett.* 22(18), 954 (1986)

44. J. R. Jr Arthur, Interaction of Ga and As_2 molecular beams with GaAs surfaces, *J. Appl. Phys.* 39(8), 4032 (1968)

45. D. G. Schlom and J. S. Harris, MBE Growth of High T_c Superconductors, in: Molecular Beam Epitaxy: Applications to Key Materials, Ed. RFC Farrow, Park Ridge, 1995, p. 505

46. Y. S. Kim, N. Bansal, and S. Oh, Crucible aperture: An effective way to reduce source oxidation in oxide molecular beam epitaxy process, *J. Vac. Sci. Technol. A* 28(4), 600 (2010)

47. Y. S. Kim, N. Bansal, and S. Oh, Simple self-gettering differential-pump for minimizing source oxidation in oxide-MBE environment, *J. Vac. Sci. Technol. A* 29(4), 041505 (2011)

48. H. T. Zhang, L. R. Dedon, L. W. Martin, and R. Engel-Herbert, Self-regulated growth of $LaVO_3$ thin films by hybrid molecular beam epitaxy, *Appl. Phys. Lett.* 106(23), 233102 (2015)

49. B. Jalan, R. Engel-Herbert, N. J. Wright, and S. Stemmer, Growth of high-quality $SrTiO_3$ films using a hybrid molecular beam epitaxy approach, *J. Vac. Sci. Technol. A* 27(3), 461 (2009)

50. P. Fisher, H. Du, M. Skowronski, P. A. Salvador, O. Maksimov, and X. Weng, Stoichiometric, nonstoichiometric, and locally nonstoichiometric $SrTiO_3$ films grown by molecular beam epitaxy, *J. Appl. Phys.* 103(1), 013519 (2008)

51. Z. Yu, Y. Liang, C. Overgaard, X. Hu, J. Curless, H. Li, Y. Wei, B. Craigo, D. Jordan, R. Droopad, J. Finder, K. Eisenbeiser, D. Marshall, K. Moore, J. Kulik, and P. Fejes, Advances in heteroepitaxy of oxides on silicon, *Thin Solid Films* 462–463, 51 (2004)

52. C. P. I. Ichimiya Ayahiko, Reflection High Energy Election Diffraction, Cambridge: Cambridge University Press, 2004

53. P. Moetakef, D. G. Ouellette, J. Y. Zhang, T. A. Cain, S. J. Allen, and S. Stemmer, Growth and properties of GdTiO3 films prepared by hybrid molecular beam epitaxy, *J. Cryst. Growth* 355(1), 166 (2012)

54. Y. Liang, W. T. Li, S. Y. Zhang, C. J. Lin, C. Li, Y. Yao, Y. Q. Li, H. Yang, and J. D. Guo, Homoepitaxial $SrTiO_3$(111) film with high dielectric performance and atomically well-defined surface, *Sci. Rep.* 5(1), 10634 (2015)

55. M. P. Warusawithana, C. Richter, J. A. Mundy, P. Roy, J. Ludwig, S. Paetel, T. Heeg, A. A. Pawlicki, L. F. Kourkoutis, M. Zheng, M. Lee, B. Mulcahy, W. Zander, Y. Zhu, J. Schubert, J. N. Eckstein, D. A. Muller, C. S. Hellberg, J. Mannhart, and D. G. Schlom, $LaAlO_3$ stoichiometry is key to electron liquid formation at $LaAlO_3$/$SrTiO_3$ interfaces, *Nat. Commun.* 4, 2351 (2013)

56. J. Goniakowski, F. Finocchi, and C. Noguera, Polarity of oxide surfaces and nanostructures, *Rep. Prog. Phys.* 71(1), 016501 (2008)

57. J. A. Enterkin, A. K. Subramanian, B. C. Russell, M. R. Castell, K. R. Poeppelmeier, and L. D. Marks, A homologous series of structures on the surface of $SrTiO_3$ (110), *Nat. Mater.* 9(3), 245 (2010)

58. R. Bachelet, F. Valle, I. C. Infante, F. Sanchez, and J. Fontcuberta, Step formation, faceting, and bunching in atomically flat $SrTiO_3$ (110) surfaces, *Appl. Phys. Lett.* 91(25), 251904 (2007)

59. J. Brunen and J. Zegenhagen, Investigation of the $SrTiO_3$ (110) surface by means of LEED, scanning tunneling microscopy and Auger spectroscopy, *Surf. Sci.* 389(1–3), 349 (1997)

60. H. Bando, Y. Aiura, Y. Haruyama, T. Shimizu, and Y. Nishihara, Structure and electronic states on reduced $SrTiO_3$ (110) surface observed by scanning-tunneling-microscopy and spectroscopy, *J. Vac. Sci. Technol. B* 13(3), 1150 (1995)

61. B. C. Russell and M. R. Castell, Reconstructions on the polar $SrTiO_3$ (110) surface: Analysis using STM, LEED, and AES, *Phys. Rev. B* 77(24), 245414 (2008)

62. Z. M. Wang, K. H. Wu, Q. L. Guo, and J. D. Guo, Tuning the termination of the $SrTiO_3$ (110) surface by Ar+ sputtering, *Appl. Phys. Lett.* 95(2), 021912 (2009)

63. F. M. Li, Z. M. Wang, S. Meng, Y. B. Sun, J. L. Yang, Q. L. Guo, and J. D. Guo, Reversible transition between thermodynamically stable phases with low density of oxygen vacancies on the $SrTiO_3$ (110) surface, *Phys. Rev. Lett.* 107(3), 036103 (2011)

64. Z. M. Wang, F. Yang, Z. Q. Zhang, Y. Y. Tang, J. G. Feng, K. H. Wu, Q. L. Guo, and J. D. Guo, Evolution of the surface structures on $SrTiO_3$ (110) tuned by Ti or Sr concentration, *Phys. Rev. B* 83(15), 155453 (2011)

65. Y. Haruyama, Y. Aiura, H. Bando, Y. Nishihara, and H. Kato, Annealing temperature dependence on the electronic structure of the reduced $SrTiO_3$ (111) surface, *J. Electron Spectroscopy and Related Phenomena* 88–91, 695 (1998)

66. S. Sekiguchi, M. Fujimoto, M. G. Kang, S. Koizumi, S. B. Cho, and J. Tanaka, Structure analysis of $SrTiO_3$ (111) polar surfaces, *Jpn. J. Appl. Phys.* 37(7), 4140 (1998)

67. S. Sekiguchi, M. Fujimoto, M. Nomura, S. B. Cho, J. Tanaka, T. Nishihara, M. G. Kang, and H. H. Park, Atomic force microscopic observation of $SrTiO_3$ polar surface, *Solid State Ion.* 108(1–4), 73 (1998)

68. H. Tanaka and T. Kawai, Surface structure of reduced $SrTiO_3$ (111) observed by scanning tunneling microscopy, *Surf. Sci.* 365(2), 437 (1996)

69. B. C. Russell and M. R. Castell, $(\sqrt{13}\times\sqrt{13})R13.9^\circ$ and $(\sqrt{7}\times\sqrt{7})R19.1^\circ$ reconstructions of the polar $SrTiO_3$ (111) surface, *Phys. Rev. B* 75(15), 155433 (2007)

70. B. C. Russell and M. R. Castell, Surface of sputtered and annealed polar $SrTiO_3$ (111): TiO_x-rich $(n \times n)$ reconstructions, *J. Phys. Chem. C* 112(16), 6538 (2008)

71. J. G. Feng, X. T. Zhu, and J. D. Guo, Reconstructions on $SrTiO_3$ (111) surface tuned by Ti/Sr deposition, *Surf. Sci.* 614, 38 (2013)

72. Z. M. Wang, F. M. Li, S. Meng, J. D. Zhang, E. W. Plummer, U. Diebold, and J. D. Guo, Strain-induced defect superstructure on the $SrTiO_3$ (110) surface, *Phys. Rev. Lett.* 111(5), 056101 (2013)

73. K. Shimoyama, K. Kubo, T. Maeda, and K. Yamabe, Epitaxial growth of $BaTiO_3$ thin film on $SrTiO_3$ substrate in ultra-high vacuum without introducing oxidant, *Jpn. J. Appl. Phys.* 40(5a), L463 (2001)

74. K. Shimoyama, M. Kiyohara, A. Uedono, and K. Yamabe, Homoepitaxial growth of $SrTiO_3$ in an ultrahigh vacuum with automatic feeding of oxygen from the substrate at temperatures as low as 370°C, *Jpn. J. Appl. Phys.* 41(3a), L269 (2002)

75. K. Shimoyama, M. Kiyohara, K. Kubo, A. Uedono, and K. Yamabe, Epitaxial growth of $BaTiO_3/SrTiO_3$ structures on $SrTiO_3$ substrate with automatic feeding of oxygen from the substrate, *J. Appl. Phys.* 92(8), 4625 (2002)

76. R. A. De Souza, V. Metlenko, D. Park, and T. E. Weirich, Behavior of oxygen vacancies in single-crystal $SrTiO_3$: Equilibrium distribution and diffusion kinetics, *Phys. Rev. B* 85(17), 174109 (2012)

77. F. M. Li, F. Yang, Y. Liang, S. Li, Z. Yang, Q. Zhang, W. Li, X. Zhu, L. Gu, J. Zhang, E. W. Plummer, and J. Guo, δ-doping of oxygen vacancies dictated by thermodynamics in epitaxial $SrTiO_3$ films, *AIP Adv.* 7(6), 065001 (2017)

78. L. D. Marks, A. N. Chiaramonti, S. U. Rahman, and M. R. Castell, Transition from order to configurational disorder for surface reconstructions on $SrTiO_3$ (111), *Phys. Rev. Lett.* 114(22), 226101 (2015)

79. H. Z. Cheng and A. Selloni, Surface and subsurface oxygen vacancies in anatase TiO_2 and differences with rutile, *Phys. Rev. B* 79(9), 092101 (2009)

80. J. Shin, A. Y. Borisevich, V. Meunier, J. Zhou, E. W. Plummer, S. V. Kalinin, and A. P. Baddorf, Oxygen-Induced Surface Reconstruction of SrRuO3 and Its Effect on the BaTiO3 Interface, *ACS Nano* 4(7), 4190 (2010)

81. L. M. Peng, Electron atomic scattering factors and scattering potentials of crystals, *Micron* 30(6), 625 (1999)

82. B. Kubota, Decomposition of higher oxides of chromium under various pressures of oxygen, *J. Am. Ceram. Soc.* 44(5), 239 (1961)

83. R. N. Song, M. H. Hu, X. R. Chen, and J. D. Guo, Epitaxial growth and thermostability of cubic and hexagonal $SrMnO_3$ films on $SrTiO_3$ (111), *Front. Phys.* 10(3), 321 (2015)

84. M. Huijben, A. Brinkman, G. Koster, G. Rijnders, H. Hilgenkamp, and D. H. A. Blank, Structure-property relation of $SrTiO_3/LaAlO_3$ interfaces, *Adv. Mater.* 21(17), 1665 (2009)

85. R. Tromp, G. W. Rubloff, P. Balk, F. K. Legoues, and E. J. Vanloenen, High-temperature SiO_2 decomposition at the SiO_2/Si interface, *Phys. Rev. Lett.* 55(21), 2332 (1985)

86. Y. W. Xie and H. Y. Hwang, Tuning the electrons at the $LaAlO_3/SrTiO_3$ interface: From growth to beyond growth, *Chin. Phys. B* 22(12), 127301 (2013)

87. W. T. Li, Y. Liang, W. H. Wang, F. Yang, and J. D. Guo, Precise control of $LaTiO_3$ (110) film growth by molecular beam epitaxy and surface termination of the polar film, *Acta Physica Sinica* 64(7), 078103 (2015)

88. I. C. Infante, J. O. Osso, F. Sanchez, and J. Fontcuberta, Tuning in-plane magnetic anisotropy in (110) $La_{2/3}Ca_{1/3}MnO_3$ films by anisotropic strain relaxation, *Appl. Phys. Lett.* 92(1), 012508 (2008)

89. J. X. Ma, X. F. Liu, T. Lin, G. Y. Gao, J. P. Zhang, W. B. Wu, X. G. Li, and J. Shi, Interface ferromagnetism in (110)-oriented $La_{0.7}Sr_{0.3}MnO_3/SrTiO_3$ ultrathin superlattices, *Phys. Rev. B* 79(17), 174424 (2009)

90. A. Roy and D. Vanderbilt, Theory of prospective perovskite ferroelectrics with double Rocksalt order, *Phys. Rev. B* 83(13), 134116 (2011)

91. J. Chang, K. Lee, M. H. Jung, J. H. Kwon, M. Kim, and S. K. Kim, Emergence of room-temperature magnetic ordering in artificially fabricated ordered-double-perovskite Sr_2FeRuO_6, *Chem. Mater.* 23(11), 2693 (2011)

92. K. Y. Yang, W. G. Zhu, D. Xiao, S. Okamoto, Z. Q. Wang, and Y. Ran, Possible interaction-driven topological phases in (111) bilayers of $LaNiO_3$, *Phys. Rev. B* 84(20), 201104(R) (2011)

93. D. Xiao, W. G. Zhu, Y. Ran, N. Nagaosa, and S. Okamoto, Interface engineering of quantum Hall effects in digital transition metal oxide heterostructures, *Nat. Commun.* 2, 596 (2011)

94. R. Mishra, J. R. Soliz, P. M. Woodward, and W. Windl, Ca_2MnRuO_6: Magnetic order arising from chemical chaos, *Chem. Mater.* 24(14), 2757 (2012)

95. F. D. M. Haldane, Model for a quantum Hall-effect without Landau-Levels – condensed-matter realization of the parity anomaly, *Phys. Rev. Lett.* 61(18), 2015 (1988)

96. D. Doennig, W. E. Pickett, and R. Pentcheva, Massive symmetry breaking in $LaAlO_3/SrTiO_3$ (111) quantum wells: A three-orbital strongly correlated generalization of graphene, *Phys. Rev. Lett.* 111(12), 126804 (2013)

97. C. R. Ma, M. Liu, C. L. Chen, Y. Lin, Y. R. Li, J. S. Horwitz, J. C. Jiang, E. I. Meletis, and Q. Y. Zhang, The origin of local strain in highly epitaxial oxide thin films, *Sci. Rep.* 3(1), 3092 (2013)

98. D. G. Schlom, L. Q. Chen, X. Q. Pan, A. Schmehl, and M. A. Zurbuchen, A thin film approach to engineering functionality into oxides, *J. Am. Ceram. Soc.* 91(8), 2429 (2008)

99. J. Liu, M. Kareev, S. Prosandeev, B. Gray, P. Ryan, J. W. Freeland, and J. Chakhalian, Effect of polar discontinuity on the growth of $LaNiO_3/LaAlO_3$ superlattices, *Appl. Phys. Lett.* 96(13), 133111 (2010)

100. J. L. Blok, X. Wan, G. Koster, D. H. A. Blank, and G. Rijnders, Epitaxial oxide growth on polar (111) surfaces, *Appl. Phys. Lett.* 99(15), 151917 (2011)

101. Y. Mukunoki, N. Nakagawa, T. Susaki, and H. Y. Hwang, Atomically flat (110) $SrTiO_3$ and heteroepitaxy, *Appl. Phys. Lett.* 86(17), 171908 (2005)

102. G. Koster, G. J. H. M. Rijnders, D. H. A. Blank, and H. Rogalla, Imposed layer-by-layer growth by pulsed laser interval deposition, *Appl. Phys. Lett.* 74(24), 3729 (1999)

103. M. Kareev, S. Prosandeev, B. Gray, J. Liu, P. Ryan, A. Kareev, E. Ju Moon, and J. Chakhalian, Sub-monolayer nucleation and growth of complex oxides at high supersaturation and rapid flux modulation, *J. Appl. Phys.* 109(11), 114303 (2011)

104. B. Dam, J. H. Rector, J. Johansson, J. Huijbregtse, and D. G. De Groot, Mechanism of incongruent ablation of SrTiO3, *J. Appl. Phys.* 83(6), 3386 (1998)

105. M. Hu, Q. Zhang, L. Gu, Q. Guo, Y. Cao, M. Kareev, J. Chakhalian, and J. Guo, Reconstruction-stabilized epitaxy of $LaCoO_3/SrTiO_3$ (111) heterostructures by pulsed laser deposition, *Appl. Phys. Lett.* 112(3), 031603 (2018)